REFRACTORY, CERAMIC, AND COMPOSITE MATERIALS

Impact of High Pressures during the Compaction of Zirconia Nanopowder on Material Structure Formation

S. E. Porozova[a], *, **, L. D. Sirotenko[a], ***, and V. O. Shokov[a], ****

[a]Perm National Research Polytechnic University, Perm, 614013 Russia
*e-mail: keramik@pm.pstu.ac.ru
**e-mail: sw.porozova@yandex.ru
***e-mail: detail@pstu.ru
****e-mail: dbnei@mail.ru

Abstract—The influence of compaction pressure during semidry compaction in a steel mold of zirconia powder partially stabilized by yttria on the phase composition and microstructure of formed compacts, as well as samples sintered at 1400°C for 2 h, is investigated. An aqueous solution of polyvinyl alcohol is selected as a temporary manufacturing binder. The yttria content in the powder synthesized according to the sol–gel technology (the deposition by an aqueous-ammonia solution from aqueous ethanol solutions of corresponding reagents with the agar-agar additive) is 3.2 mol % according to the X-ray fluorescent analysis data. The results of studying the compacts and sintered samples by Raman spectroscopy, optical microscopy, and atomic force microscopy are presented. It is established that an increase in their density is not monotonic. There is the critical range of compaction pressures $P = 400-450$ MPa, in which the porosity, pore shape and sizes, microstructure, and phase composition of the material vary abruptly. A monoclinic phase, the content of which varies upon varying P, is fixed in compacted samples along with tetragonal zirconia. Material grain grinding is associated with the destruction of agglomerates and actively occurs in range $P = 350-550$ MPa. A similar effect when studying the compaction process of nanopowders of zirconia is also noted by other researchers, who assumed that the response of the nanopowder system on the pressure effect is associated with the influence on the aqueous component (the temporary manufacturing binder in this case) and is caused by the transition of one form of water into another one at $10-25$°C and a pressure of $400-700$ MPa.

Keywords: compaction pressure, nanopowder, zirconia, porosity, microstructure, phase composition

DOI: 10.3103/S1067821220020108

INTRODUCTION

Currently, numerous methods of fabricating both metallic and ceramic nanopowders are developed [1–3]. However, not nanopowder itself, but the bulk porous or compact ware based on it is of interest in the overwhelming majority of cases. When fabricating it, the advantages of the nanostructured materials are retained if possible. The formation of wares from nanopowders is a rather complex problem because the compact or porous billet always inherits the structural features of the initial powder [4, 5]. To attain the optimal characteristics of materials, nanopowders formed by various methods require various compaction conditions.

The authors of [4–7] studied the dry compaction of nanopowders with the application of the ultrasonic impact. The developed technology makes it possible to fabricate complexly shaped wares with high physicomechanical characteristics. Herewith, nanopowders used for the compaction should have good fluidity such as that inherent, for example, in plasmachemical powders [8].

Powders fabricated by chemical methods have low fluidity and are prone to poorly controllable aggregation, while high interparticle friction considerably complicates their compaction [9]. Nevertheless, the synthesis, for example, of various variants of sol–gel technology is used rather often because it makes it possible to vary the properties of powders. For example, the fabrication method of nanopowders by the reverse precipitation by ammonia from aqueous alcohol solutions of salts with polymer additives, which was developed at the Scientific Center of Powder Materials Science (Perm National Research Polytechnic University, Perm) [10], makes it possible not only fabricate powders with a narrow particle-size distribution, but also, when varying the polymer additive, vary the particle size. The compaction of such powders can be performed by semidry uniaxial compaction when using the temporary manufacturing binder and preliminary agglomeration [11].

The goal of our work is to investigate the influence of the compaction pressure on the phase composition and microstructure of zirconia samples stabilized by
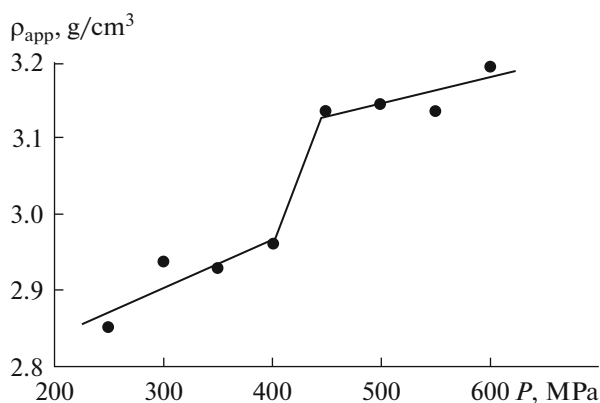
ρ_{app}, g/cm^3

Fig. 1. Dependence of apparent density of compacted samples on the compaction pressure.

yttria. The zirconia powder stabilized by 3.5 mol % Y_2O_3 (the calculated amount for the synthesis) was used as the main object of the investigation.

EXPERIMENTAL

The powder was fabricated under laboratory conditions according to sol–gel technology.

The sol preparation and its coagulation were performed according to the procedure developed earlier from aqueous-ethanol solutions of salts with the addition of water-soluble polymer—agar-agar [10]. Reagents of chemical purity and analytical grade were used for the synthesis, notably, $ZrOCl_2 \cdot 8H_2O$, $Y(NO_3)_3 \cdot 6H_2O$, 25% aqueous ammonia solution, natural agar-agar polymer, 96% ethanol (C_2H_5OH), and distilled water. The precipitate was calcined at 550°C. The specific powder surface determined according to the thermal desorption method was 67 m^2/g, while the particle size calculated by the specific surface was 15 nm.

To improve compaction [11], mechanical treatment of the powder was performed using a SAND planetary mill in chalcedony drums with chalcedony milling bodies at a revolution rate of 160 rpm for 30 min. Activation was performed in an aqueous medium with the addition of 0.5 wt % agar-agar (with the weight ratio balls : powder : water = 2 : 1 : 1).

The formation was performed by steel cold semidry uniaxial compaction in a steel mold under pressure $P = 200–800$ MPa with an interval of 50 MPa. The use of a narrower interval lowers the reliability of results because of an insufficient accuracy of the compacting equipment. The 4% aqueous solution of polyvinyl alcohol was used as a temporary manufacturing binder. The binder was removed upon heating samples to 800°C without holding. Sintering was performed in air medium at 1400°C with holding of 2 h.

The yttria content was determined using an EDX-800HS X-ray fluorescent spectrometer (Shimadzu, Japan). The apparent density of compacts was evaluated by the weight ratio and geometrically determined volume of the samples. The open porosity of sintered samples was investigated according to *GOST* (State Standard) *2409–2014*.

Images of compacted samples after annealing of the temporary manufacturing binder [12], which were fabricated using an Axiovert 40MAT inverted metallographic microscope of reflected light (Carl Zeiss, Germany), were analyzed using the VideoTesT-Master:Struktura program. The total porosity was determined and the pore distribution by size, average and equivalent diameters, and the form factor were investigated.

The phase analysis of fabricated samples was evaluated by Raman spectroscopy using a Senterra multifunctional spectrometer (Bruker, Germany) at the emitting laser wavelength of 532 nm [13]. The content of a monoclinic modification was determined indirectly by the ratio of intensities of peaks of a monoclinic and tetragonal modifications [14, 15] according to the following formula:

$$f_m = [I_m^{181} + I_m^{192}]/[k(I_t^{148} + I_t^{264}) + I_m^{181} + I_m^{192}],$$

where upper indexes are referred to the combination shift of characteristic peaks, while the lower indexes, correspondingly, show the peak attribution to a monoclinic (m) or tetragonal (t) phase; coefficient $k = 0.97$.

To reveal the surface microstructure, microslices of sintered samples were subjected to high-temperature etching at 1250°C for 30 min in air atmosphere [16].

The surface microstructure of microslices of sintered samples was investigated by atomic force microscopy using a Solver Next scanning probe microscope (NT-MDT, Russia). The data were treated using a Gwyddion software. The surface microstructure was investigated using a VEGA3 (TESCAN, Czech Republic).

The crack-resistance tests of samples were performed by the indentation of the polished surface of microslices by a Vickers pyramid using a TU-2137 hardness meter under a load of 98.1 N. The length of diagonals of the imprint and cracks forming in its angles were measured using an Axiovert 40MAT digital inverted microscope (Carl Zeiss, Germany) with the visualization and documentary photograph system. The crack-resistance coefficient (K_{Ic}) was determined according to the Niihara formula [17, 18].

RESULTS AND DISCUSSION

Figure 1 shows the dependence of the apparent density of compacted samples on the compaction pressure. Confidence intervals of measured quantities are ±0.03–0.04. It is noteworthy that the results are approximated well by two straight lines, and a consid-

Table 1. Results of analysis of surface images of compacted samples

Sample no.	P, MPa	P_{tot}, %	Pore content, %		
			$d_{av} = 0.3-3.0$ μm	$d_{eq} = 0.7-2.3$ μm	Shape factor is 0.91−1.00, rel. units
I	350	18	58	53	72
II	550	16	72	64	81

* After annealing the temporary manufacturing binder.

erable variation in density is fixed in compaction pressure range $P = 400-450$ MPa.

Similar results are found for several series of the samples with the content of the stabilizing zirconia additive of 3−4 mol %. The deviations from the straight line of compact density at $P = 300$ and 550 MPa were not taken into account because their confidence intervals are overlapped with those of neighboring points.

The porosity and phase composition were studied for compacted samples I ($P = 350$ MPa) and II ($P = 550$ MPa) as typical representatives of their groups. The temporary manufacturing binder was preliminarily annealed at 800°C. The results of an analysis of images recorded using an Axiovert 40MAT inverted reflected-light metallographic microscope are presented in Table 1. The analysis is performed using the VideoTest-Master:Struktura program. Despite an insignificant decrease in total porosity (P_{tot}) with an increase in the compaction pressure, we can note an increase in the content of fine pores ($d_{av} = 0.7-3.0$ μm) from 58 to 72% of their total amount, a decrease in the equivalent diameter of pores (d_{eq}), and an increase in amount of pores with shape close to spherical.

The experiments were performed for nonsintered samples. The substantial difference in the results of measuring the apparent density (Fig. 1) and, correspondingly, apparent porosity by the geometric method[1] and porosity (gap) (Table 1) point to the fact that compact pores are mainly very fine (<0.3 μm) and are not determined using a metallographic microscope.

The phase composition was evaluated by the Raman spectroscopy. As far as the main phases in materials based on zirconia are monoclinic, tetragonal transformable, tetragonal untransformable, and cubic [19], the content of a monoclinic phase is very important. The possibility of its conservation and/or formation in the wares determines both a decrease in strength

[1] The hydrostatic weighing method is unsuitable for compacted samples.

up to the fracture and the transformation strengthening effect, which, according to the commonly accepted opinion [20], is the cause of an increased crack resistance of materials made of zirconia.

The monoclinic phase content in the initial powder according to Raman spectroscopy data was 23%. The peaks of tetragonal and monoclinic modifications are identified in the Raman spectra of both compacted samples I and II, and the peaks of the monoclinic modifications are most intense. Herewith, the shift by 3−4 cm^{-1} of wave numbers [14], which characterize the highest peak intensity, can be caused by distinctions in the preparation and recording of the samples.

Figure 2 shows the fragments of the Raman spectra of compacted samples. Figure 2 shows the peaks in region $\nu = 120-350$ cm^{-1}, the ratio of absolute intensities of which is used when determining the content of the monoclinic modification [14]. The amount of a monoclinic modification in sample I was 22% (almost the same as in the initial powder), and in sample II it was 16%.

The presence of the cubic modification, which is presented by one line in the Raman spectra [13], can be fixed only indirectly upon the factorization according to the Levenberg−Marquardt algorithm. Figures 2b and 2c show the factorization using the Gaussian function. The factorization was performed in a semiautomatic mode, when the number of peaks usually weakly depends on the operator, and the main role is played by the device software.

In the first case, the factorization had led to two peaks with wave numbers 614 and 639 cm^{-1} and, in the second case, to three peaks with $\nu = 604$, 630, and 640 cm^{-1}. The integral intensity of peaks was 35 and 65% for sample I and 9, 49, and 42% for sample II.

The tetragonal shape of polycrystalline zirconia is characterized by peaks with $\nu = 641$, 473, 260, and 146 cm^{-1} [13] and the cubic one has peaks with 620−630 cm^{-1}. The peak of the monoclinic modifications is fixed closer to 600 cm^{-1} according to the data of various researchers [13].
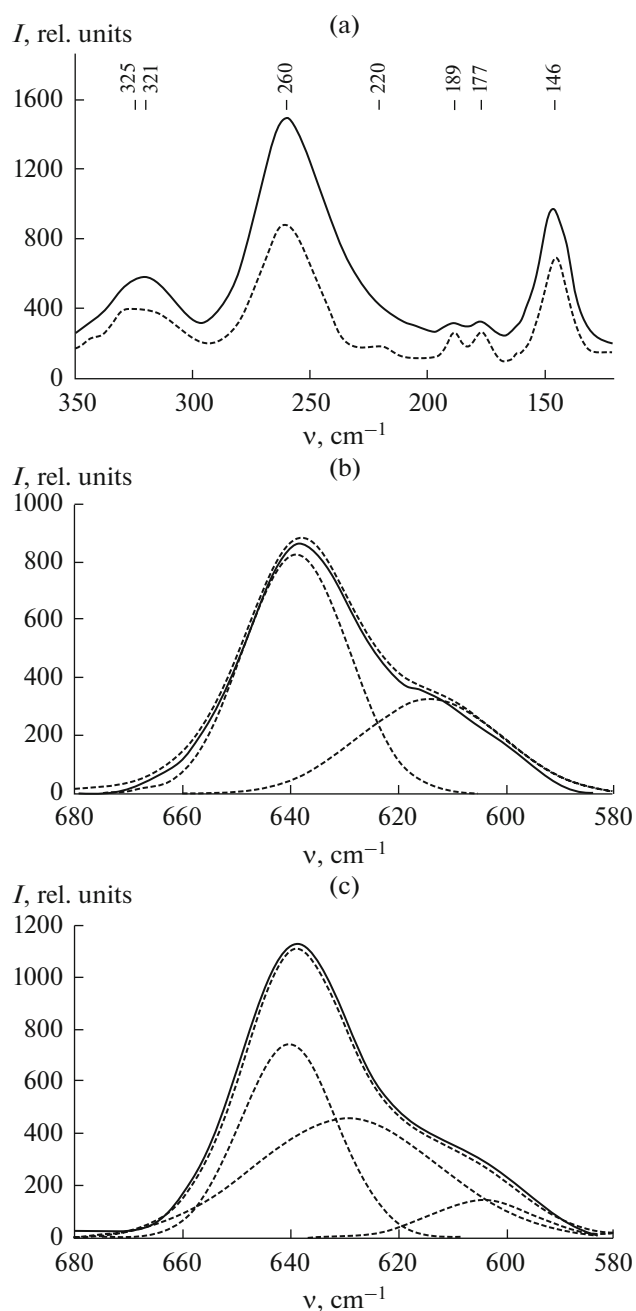
Fig. 2. Fragments of Raman spectra of compacted samples I and II after removing the temporary binder. (a) Peaks used when calculating the content of the monoclinic modification and (b) and (c) factorization of spectra of samples I and II, respectively. Dotted lines note the peaks found after spectrum factorization and the solid line is the summary curve.
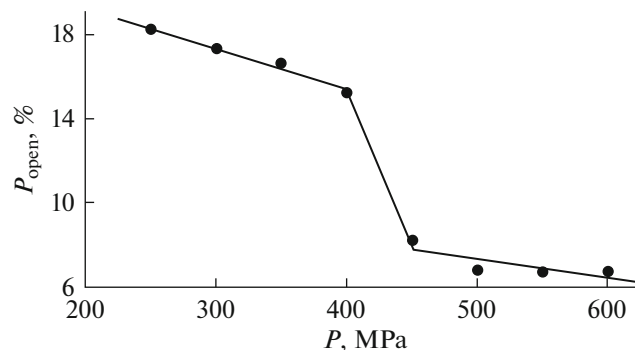
Fig. 3. Dependence of open porosity of sintered samples on the compaction pressure.

cubic or tetragonal untransformable (t') phases, the lattice constants of which are almost identical [19, 21, 22].

The yttria content in both billets was 3.2–3.3 mol % according to X-ray fluorescent analysis data.

Further investigations were performed for sintered samples. The Raman spectroscopy data evidence the absence of a monoclinic phase in them irrespective the compaction pressure of billets.

Table 2 shows the results of the analysis for images of microslices of sintered samples performed using the VideoTest-Master:Struktura program. The variation in the total porosity is nonmonotonic, and its minimum at a compaction pressure of 500 MPa also corresponds to the maximal content of pores with $d_{av} < 4.0\,\mu m$ and pores with a shape close to spherical.

Figure 3 shows the dependence of open porosity for sintered samples (according to *GOST 2409–2014*) on the compaction pressure. An almost twofold decrease in porosity is noted in range $P = 400–450$ MPa in both cases (Table 2, Fig. 3), although we speak about its different types determined by different methods. Substantial variations in the pore size and shape are fixed in the same pressure range. The data of microslice analysis images evidence that the samples compacted at 350 and 500 MPa also enter the instability region.

Figure 4 shows SEM images of the surface of microslices for sintered samples ($P = 350$ and 700 MPa) recorded using a VEGA3 TESCAN scanning electron microscope under a magnification of 50000×. Recording was performed after high-temperature etching at 1250°C for 30 min. A decrease in the grain size with an increase in the compaction pressure is fixed. It is also evident that $P = 700$ MPa does not provide the complete destruction of agglomerates in zirconia.

The grain size was calculated by profilograms of AFM images using the Gwyddion software. The average size of grains compacted at 400 MPa was 307 ± 22 nm, and at 500 MPa—204 ± 47 nm. Refining the material grains is associated with the destruction of

Thus, the phase composition of samples I and II under compaction pressures under study is different. The content of the monoclinic modification decreases with an increase in P according to the Raman spectroscopy data, apparently due to the appearance of the

Table 2. Results of an analysis of images for microslices of sintered samples

P, MPa	P_{tot}, %	Pore content, %		
		$d_{av} = 0.3{-}4.0$ μm	$d_{eq} = 0.3{-}4.0$ μm	Shape factor is 0.91–1.00, rel. units
250	24	66	70	72
300	28	63	64	70
350	16	74	79	79
400	26	62	65	70
450	12	74	75	84
500	9	76	79	86
550	16	69	71	81
600	16	70	71	83

agglomerates and actively proceeds in the range $P = 350{-}550$ MPa. The minimal grain size under a compaction pressure of 650 MPa already almost corresponds to the particle size of the initial powder.

The authors of [9], who noted a similar effect, assume that the response of the nanopowder system in the pressure impact is associated with the influence on the aqueous component (the temporary manufacturing binder in this case) and is conditioned by the transition of one water form into another [23, 24]. This transition in a temperature range of 10–25°C is fixed under a pressure of 400–700 MPa and leads to a sub-stantial variation in the behavior of hydrogen bonds that are able to actively affect nanopowders [9]. Microsized powders are not as sensitive to such impacts.

The crack resistance coefficient (K_{Ic}) is considered one of the main operational characteristics of zirconia-based ceramics. Figure 5 shows the plot of its dependence on the compaction pressure of the zirconia nanopowder. An increase in K_{Ic} with an increase in the compaction pressure is noted. Their largest spread is fixed in range $P = 400{-}450$ MPa.
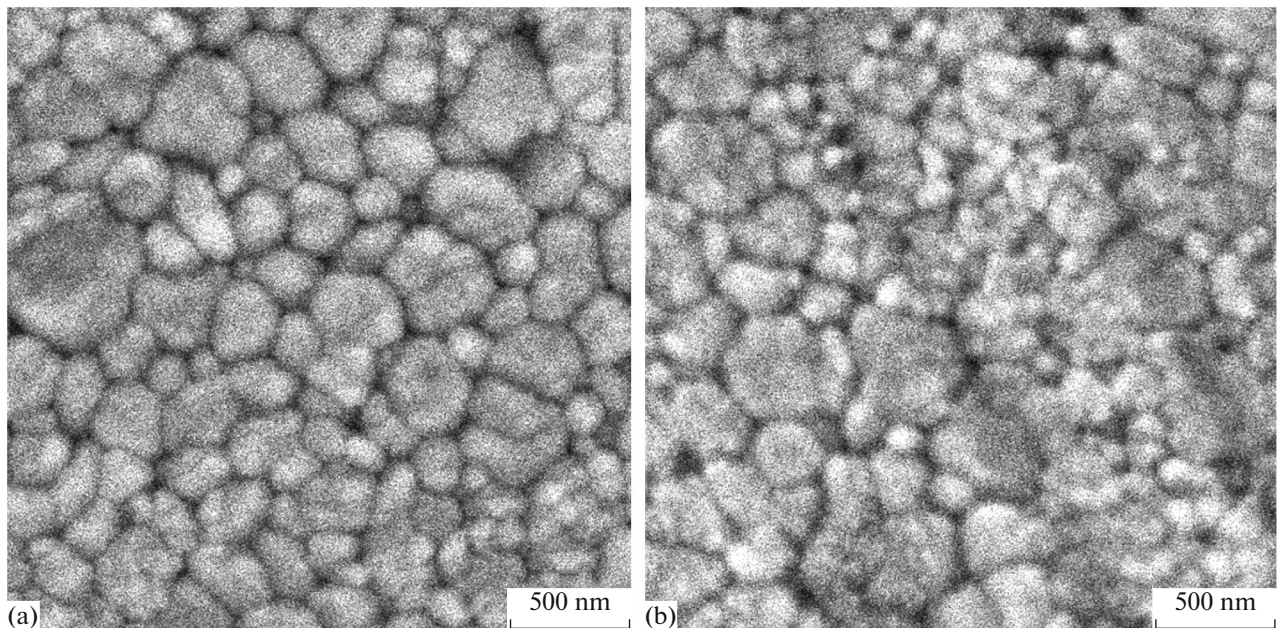
Fig. 4. Fragments of SEM images of zirconia microslices. (a) $P = 350$ and (b) 700 MPa. Magnification 50000×.
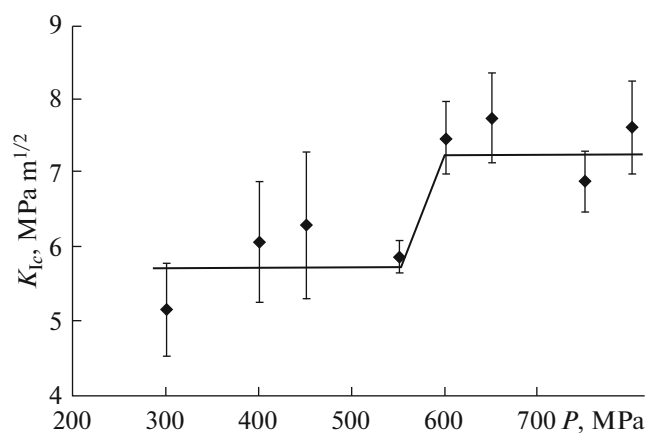
Fig. 5. Dependence of crack resistance of sintered samples on the compaction pressure.

CONCLUSIONS

The influence of pressure during the semidry compaction of zirconia nanopowder stabilized by 3.2 mol % yttria in a steel mold on some characteristics of compacts and sintered materials is investigated. It is established that an increase in the density of compacts and sintered samples is not monotonic. There is critical range $P = 400-450$ MPa, in which a considerable variation in porosity, shape, and pore sizes of the material takes place.

It is revealed that the phase composition depends on the compaction pressure only for compacts. All sintered samples contain the tetragonal phase exclusively according to Raman spectroscopy data. A decrease in the grain size occurs with an increase in the compaction pressure due to the destruction of agglomerates during compaction, and an increase in the ceramic crack-resistance coefficient is observed.

CONFLICT OF INTEREST

The authors declare that they have no conflict of interest.

REFERENCES

1. Mondal, A. and Ram, S., Reconstructive phase formation of ZrO_2 nanoparticles in a new orthorhombic crystal structure from an energized porous $ZrO(OH)_2 \cdot H_2O$ precursor, *Ceram. Int.,* 2004, vol. 30, pp. 239–249. https://doi.org/10.1016/S0272-8842(03)00095-6

2. Ivanov, Yu.F., Tumanov, Yu.N., Dedov, N.V., and Khasanov, O.L., Structure and phase composition of nano-structural powder on the base of zirconium dioxide made by methods of plasma-chemical synthesis, *Fiz. Khim. Obrab. Mater.,* 2012, no. 5, pp. 37–45.

3. Thakare, V., Progress in synthesis and applications of zirconia, *Int. J. Eng. Res. Dev.,* 2012, vol. 5, no. 1, pp. 25–28.

4. Karban', O.V., Khazanov, E.N., Khasanov, O.L., Salamatov, E.I., and Goncharov, O.Yu., Heredity and modification of ZrO_2 nano-structural ceramics during production, *Perspekt. Mater.,* 2010, no. 6, pp. 76–85.

5. Popov, V.V., Petrunin, V.F., Chzhu, Kh., Khasanov, O.L., and Dvilis, E.S., The way for researching regularities of pressing ZrO_2 powders under ultrasonic influence, *Ogneupory Tekh. Keram.,* 2007, no. 11, pp. 17–23.

6. Dvilis, E.S., Chartpuk, P., Khasanov, O.L., Sokolov, V.M., and Eshetov, B.A., Analytical and model optimization of kinematic schemes of uniform-dense pressing of powder materials, *Izv. Tomsk. Politekh. Univ.,* 2013, vol. 323, no. 2, pp. 49–55.

7. Khasanov, O.L., Structure and properties of the zirconium ceramics manufactured by ultrasonic compaction of nano-powders, *Konstr. Kompoz. Mater.,* 2007, no. 1, pp. 60–72.

8. Matsumoto, R.L.K., Analysis of powder compaction using a compaction rate diagram, *J. Am. Ceram. Soc.,* 1990, vol. 73, no. 2, pp. 465–468. https://doi.org/10.1111/j.1151-2916.1990.tb06539.x

9. Konstantinova, T.E., Danilenko, I.A., and Gorban', O.A., Effects of high pressure in nano-dimensional powder systems on the base of zirconium dioxide, *Fiz. Tekh. Vys. Davlenii,* 2014, vol. 24, no. 2, pp. 67–85.

10. Antsiferov, V.N., Porozova, S.E., and Kul'met'eva, V.B., Effect of water-soluble polymer additives on the phase composition and size of zirconia particles during precipitation from salt solutions, *Glass Phys. Chem.,* 2012, vol. 38, no. 3, pp. 322–326.

11. Zigan'shin, I.R., Porozova, S.E., Karmanov, V.I., Torsunov, M.F., and Hafizova, R.M., Change in the characteristics of the industrial powder of zirconium oxide and materials based on it by mechanochemical activation, *Russ. J. Non-Ferrous Met.,* 2010, vol. 51, no. 4, pp. 337–341.

12. Krasnyi, B.L., Tarasovskii, V.P., Krasnyi, A.B., and Omarov, A.Yu., Quantitative analysis of ceramics pore structure by means of SEM-image computer analysis, *Refract. Ind. Ceram.,* 2013, vol. 54, no. 4, pp. 331–335. https://doi.org/10.1007/s11148-013-9604-9

13. Ghosh, A., Suri, A.K., Pandey, M., Thomas, S., Rama Mohan, T.R., and Rao, B.T., Nanocrystalline zirconia-yttria system—a Raman study, *Mater. Lett.,* 2006, vol. 60, pp. 1170–1173.

14. Liang, B., Ding, C., Liao, H., and Coddet, C., Study on structural evolution of nanostructured 3 mol % yttria stabilized zirconia coatings during low temperature ageing, *J. Eur. Ceram. Soc.,* 2009, vol. 29, pp. 2267–2273.

15. Porozova, S.E., Kul'met'eva, V.B., Zigan'shin, I.R., and Torsunov, M.F., Comparative characteristic of results for determining monoclinic phase content in zirconium dioxide, *Vopr. Materialoved.,* 2010, no. 1 (61), pp. 46–52.

16. Kurogi, Y., Recent trends in dry etching, *Thin Solid Films,* 1982, vol. 92, nos. 1–2, pp. 33–40. https://doi.org/10.1016/0040-6090(82)90185-7

17. Gogotsi, G.A. and Bashta, A.V., Investigation of a ceramic in indentation of a Vickers diamond pyramid, *Strength Mater.,* 1990, vol. 22, no. 9, pp. 1306-1313.

18. Gogotsi, G.A., Dub, S.N., Lomonova, E.E., and Ozersky, B.I., Vickers and knoop indentation behavior of cubic and partially stabilized zirconia crystals, *J. Eur. Ceram. Soc.,* 1995, vol. 15, pp. 405−413.

19. Viazzi, C., Bonino, J.-P., Ansart, F., and Barnabé, A., Structural study of metastable tetragonal YSZ powders produced via a sol−gel rout, *J. Alloys Compd.,* 2008, vol. 452, no. 2, p. 377383.
https://doi.org/10.1016/j.jallcom.2006.10.155

20. Kim Sung-Dai and Hwang Kyu-Seog, Crystallinity, microstructure and mechanical strength of yttria-stabilized tetragonal zirconia ceramics for optical ferrule, *Mater. Sci. Appl.,* 2011, no. 2, pp. 1−5.
https://doi.org/10.4236/msa.2011.21001

21. Sobol, A.A. and Voronko, Yu.K., Stress-induced cubic-tetragonal transformation in partially stabilized ZrO_2: Raman spectroscopy study, *J. Phys. Chem. Solids,* 2004, vol. 65, no. 6, pp. 1103−1112.
https://doi.org/10.1016/j.jpcs.2003.11.038

22. Hemberger, Y., Wichtner, N., Berthold, C., and Nickel, K.G., Quantification of yttria in stabilized zirconia by Raman spectroscopy, *Int. J. Appl. Ceram. Technol.,* 2016, vol. 13, no. 1, pp. 116−124.
https://doi.org/10.1111/ijac.12434

23. Kawamoto, T., Ochiai, S., and Kagi, H., Changes in the structure of water deduced from the pressure dependence of the Raman OH frequency, *J. Chem. Phys.,* 2004, vol. 120, no. 13, pp. 5867−5870.
https://doi.org/10.1063/1.1689639

24. Pershin, S.M., Konovalov effect in aqueous solutions in low-concentration aqueous solutions: The role of ortho/para spin isomers of water, *Dokl. Phys. Chem.,* 2014, vol. 455, no. 1, pp. 37−40.
https://doi.org/10.7868/S0869565214070123

Translated by N. Korovin